Journal of Volcanology and Geothermal Research 186 (2009) 361–378

Contents lists available at ScienceDirect

Journal of Volcanology and Geothermal Research

journal homepage: www.elsevier.com/locate/jvolgeores

Internal vs. external forcing in shallow marine diatreme formation: A case study from the Iblean Mountains (SE-Sicily, Central Mediterranean)

Ines Suiting *, Hans-Ulrich Schmincke [1]

Leibniz-Institute of Marine Sciences IFM-GEOMAR, Research Division 4: Dynamics of the Ocean Floor, Wischhofstr. 1-3, 24148 Kiel, Germany

ARTICLE INFO

Article history:
Received 26 January 2009
Accepted 20 July 2009
Available online 30 July 2009

Keywords:
diatreme
shallow marine eruption
internal forcing
pre-fragmentation
juvenile magmatic lapilli

ABSTRACT

A model of diatreme evolution in a shallow marine setting is based on a multi-disciplinary analysis of diatremes in the Iblean Mountains (Sicily). The approach includes stratigraphic, volcanological, structural, petrologic and compositional data. We invoke a complex interplay of internal (rapid ascent and pyroclastic fragmentation of a volatile (CO_2)-rich nephelinitic magma at depth) and external factors. These comprise hydroclastic explosions due to near-surface interaction of the rising particle/volatile mixture with seawater and water-saturated lime mud. Other external factors contributing to diatreme formation include regional and local tectonics (graben formation in pull-apart motion) combined with lateral pipe enlargement by bedrock-spalling and radial block subsidence into the diatreme pipe. We suggest that fragmentation of volatile-rich magma due to internal eruption forcing was fundamental in the formation of the Iblean shallow marine diatremes. Internal and external factors may act to a variable degree, however, during diatreme evolution in general.

1. Introduction

Diatremes – conically shaped breccia-filled pipes – are volcanic subsurface structures extending as deep as 2500 m below the surface (Hearn, 1968; Dawson, 1980).

The classic explanation for the formation of diatremes with kimberlitic composition invokes high velocity gas/particle mixtures drilling their way through the lithosphere (Clement, 1982; Clement and Reid, 1989; Field and Scott Smith, 1999; Skinner and Marsh, 2004). This model is based largely on the presence of diamonds – suggesting very high ascent velocities – and the inferred high concentration of volatiles especially CO_2 and lesser H_2O in the host magma, as reflected in the mineralogy (phlogopite) and/or rock composition (ultramafic, low viscosity magmas). Interaction of rising magma and external water and downward migrating of the explosion focus has been postulated by Lorenz and coworkers (Lorenz, 1985; Kurszlaukis, 1998; Kurszlaukis et al., 1998; Lorenz and Kurszlaukis, 2007; Kurszlaukis and Lorenz, 2008; Table 1). Current models of pyroclastic kimberlite diatreme formation (Sparks et al., 2006; Wilson and Head, 2007; Cas et al., 2008a; Table 1) comprise several stages of diatreme enlargement and infill and invoke pyroclastic fragmentation processes possibly accompanied by minor phreatomagmatic activity.

Although kimberlite pipes have been studied most thoroughly for obvious reasons, similar diatreme pipes are also known to form the subsurface continuation below tephra ring/maar-type volcanoes, mafic host magmas being generally of less extreme composition but nevertheless commonly of silica-undersaturated mafic composition strongly implying that composition of the magmas and their volatiles are a major factor in diatreme formation.

Many models of kimberlite diatreme formation are based on drill cores and surficial outcrops representing a cross-section several hundred meters below the eruptive surface (e.g. Hearn, 1968; Skinner and Marsh, 2004). Evidence for surface volcanic activity has been eroded above nearly all diatremes, a major handicap in developing well-documented models for their formation for more than half a century. Evidence to reconstruct surfacial eruptive and magma fragmentation processes must thus be necessarily limited. In the absence of surface evidence in form of a tephra ring, the corner stones of discussions on diatreme genesis in general include (1) presence of a deep-reaching pipe; (2) structures and textures of the clastic, largely volcanic fill; (3) abundance of mantle-derived xenoliths; and (4) mafic, silica-undersaturated host magma composition. The Costa Giardini Diatreme (CGD) (Iblean Mountains, Sicily), one of the best-exposed diatremes known, while satisfying all of these criteria, has the great advantage of harboring several salient features that allow to reconstruct evolution of one type of diatreme in unusual detail. Three of the major assets of the CDG are: (1) a well-exposed tephra ring with intercalated patch reefs suggesting diatreme evolution over many hundreds if not thousands of years; (2) unequivocal formation of the diatreme beneath a water cover of a few tens of meters; and (3) local and regional structural deformation concomitant with diatreme evolution. A presentation of these aspects forms the bulk

* Corresponding author. Home office: Am Brinkhof 29, 33813 Oerlinghausen, Germany. Tel.: +49 5202 977030; fax: +49 5202 977032.
E-mail addresses: ines.suiting@t-online.de (I. Suiting), h-u.schmincke@t-online.de (H.-U. Schmincke).
[1] Tel.: +49 431 600 2652.

0377-0273/$ – see front matter © 2009 Elsevier B.V. All rights reserved.
doi:10.1016/j.jvolgeores.2009.07.013

Table 1
Comparison of the CGD Model and other models of diatreme formation.

Evolution and volcanic phases	Lorenz (1985)	Clement and Reid (1989)	Sparks et al. (2006)	Wilson and Head (2007)	Cas et al. (2008a)	CGD
	Top downwards	Bottom upwards	Top downwards	Bottom upwards, followed by downward propagating decompression wave	Bottom upwards (tip crack propagation and hydraulic fracturing)	Synchronous activity at different levels in several vent locations, enlarging the entire subsurface structure laterally
Phases			4	6	6	5
Initial phase	Magma/water contact at the surface, open system, phreatomagmatic eruptions.	Closed system, precursor embryonic pipe within 0.5 km below surface, precursory to surface breakthrough adiabatic expansion of volatiles, hydraulic fracturing, magmatic stoping, intrusion, brecciation, spalling, slumping.	*Stage 1* Surface eruptions due to high volatile content, exit condition is overpressured and initiates crater and pipe formation.	*Stage 1* Deep source dike-propagation and CO_2 segregation. *Stage 2* Dike/fluid particle mixture ascent and wall fracturing. *Stage 3* Dike-tip of CO_2 fluid breaks the surface forms linear crushed zone of country rock; vulcanian explosion with dominantly country rock debris.	*Stage 1* Magma uprise a fluid propagation through the crust and conduit formation. *Stage 2* Vent opening by initial major ballistic gas explosion. Apron of country rock debris around the vent.	*Phase 1* Precursor lava flow, hydroclastic activity due to first (?) magma/water contact, granulation of magma at the surface. Eruptive break and closure of the volcanic system by water sediment slurry. *Phase 2* Initial doming; bedrock fracturing at depth by fluid particle mixture drilling its way upward. Explosive outburst of bedrock and lime-mud with minor volcanic particles (ca. 20 vol.%) due to high volatile pressure in the closed system. Magmatic pre-fragmentation enforced by phreatomagmatic processes at the surface. Infill of pipe by collapse of eruption column.
Enlargement, subsidence and filling	Subsidence of the explosion level and collapse into the excavated root zone	After surface breakthrough spalling, fluidization and collapse as gas velocity wanes and fluidized system deflates.	*Stage 2* Subsurface fragmentation due to underpressure (lithostatic pressure >pressure of erupting mixture) in the evolving pipe, undermining of overlying rocks (erosive stage). Pipe deepening and widening, fluidization. *Stage 3* When exit pressure = atmosphere, ejecta become trapped and the pipe fills.	*Stage 4* Depressurization causes imploding walls and gas venting: begin of diatreme formation. Disruption of magma and formation of magma droplets by surface tension; plinian plume. Stage 5 Upward wave of fluidization enlarges diatreme; pyroclast acceleration. Vent clogging reduces pyroclast escape route	*Stage 3* Waxing phase of erosion; vent clearing, reaming and sculpting. No deposition in vent. *Stage 4* Waning fountain of degassed magma and in-vent column collapse.	*Phase 3* Enlargement of the partly clogged diatreme and the complex tephra ring by repeated vent migration and new pipe development. Bedrock fragmentation contemporaneously at different levels of the subsurface structure. *Phase 4* Radial dike intrusion, scoria cone. Subsidence of diatreme fill and radial bedrock blocks. Debris flows into the diatreme.
Post-eruptive phase			*Stage 4* Post-emplacement hydrothermal alteration	*Stage 6* Post-eruption crater-lake formation and alteration	*Stage 5* Post-eruption infilling of vent by resedimentation, alteration by vapour phase streaming through the fill, intrusion of degassed magma. *Stage 6* Ingress of meteoric water and ongoing diagenetic alteration	*Phase 5* Post-eruptive lagoon with coral growth and diatomite formation.
Eruption forcing	Exclusively external (magma/water interaction)	Internal forcing of precursor subsurface processes, external (phreatomagmatic) processes at the surface possible	Internal forcing of initial surface processes, interplay of gravitational and internal forcing during Stages 2 and 3.	Internal forcing of precursor subsurface processes, external (phreatomagmatic) processes at the surface possible	Internal forcing dominates; magma/water interaction possible, but minimized due to rapid chilling (large pressure reduction) of the magmatic foam (fluid/particle mixture)	Complex interplay of internal and external forcing to varying degree throughout all volcanic phases. External factors dominating surfacial transport processes. Volatile exsolution at depths responsible for subsurface processes as fast magma uprise, and pre-fragmentation of magma.

of the subsequent discussion. As in other models previously proposed, no entirely coherent mode of origin and temporal succession of processes can be presented, but some aspects are now better constrained.

2. Regional setting

2.1. The Upper Miocene diatremes of the Iblean Mountains

In the Monti Iblei (Sicily), late Miocene alkali basaltic to nephelinitic and minor tholeiitic lavas were erupted in a shallow marine environment of a semi-consolidated carbonate platform in a complex convergent to transtensional tectonic setting (Carlentini Fm., Grasso et al., 1982; Schmincke et al., 1997). Of 11 Iblean Late Miocene eruptive centers previously called diatremes (Carbone and Lentini, 1981) we have been able to verify only 4. All of these are nephelinitic in composition and concentrated in the southeastern area of the Miocene volcanic field. Most other volcanic centers in the area, many poorly-exposed, are lava flows, scoria cones and bedded tephra.

Two of the three shallow marine diatremes (Costa Giardini (CGD) and Cozzo Molino (CMD), all well-exposed (Fig. 1) are preserved in diatreme fill and associated tephra ring facies. Only the diatreme fill is exposed at the strongly eroded Masseria D' Ingegna diatreme (MID). These diatremes show strikingly similar sedimentological and volcanological characteristics strongly implying basically similar modes of origin. Here we concentrate on sedimentological, structural and compositional characteristics and inferred eruption dynamics of the best-exposed volcanic complex, the CGD (Suiting, 2004).

The steep semicircular morphological depression of the CGD (ca. 800 m diameter at the rim) east of the town of Sortino is open to the south towards the Anapo river valley (Fig. 2). The diatreme is bound by limestone walls exposed for some 100 m below pre-eruptive seafloor at which depth the diameter of the funnel still measures ca. 600 m across. Volcaniclastic diatreme fill hides the diatreme wall below.

The CGD shows some essential characteristics common to class 1 kimberlite diatremes of Skinner and Marsh (2004) postulated to have formed by essentially pyroclastic rather than phreatomagmatic processes: (1) a funnel-shaped pipe; (2) smooth relic planes of bedrock sloping inward at 30–45° resembling a shallow flared crater zone in the uppermost 150 m of the diatreme; (3) large blocks of country rocks (olistoliths; floating reefs, Clement, 1982) sunk into the pipe; (4) abundant bedrock clasts (30–80 vol.%) and ubiquitous peridotite xenoliths in the volcaniclastic sediments; and (5) abundant pelletal and composite lapilli (Bednarz and Schmincke, 1990) (corresponding to "cored juvenile pelletal lapilli" of Cas et al., 2008b and pelletal clasts of Brown et al., 2009).

Features more common to pyroclastically-formed class 2 kimberlite diatremes of Skinner and Marsh (2004) include:

(1) Many glassy lapilli in the tephra deposits are irregularly shaped.

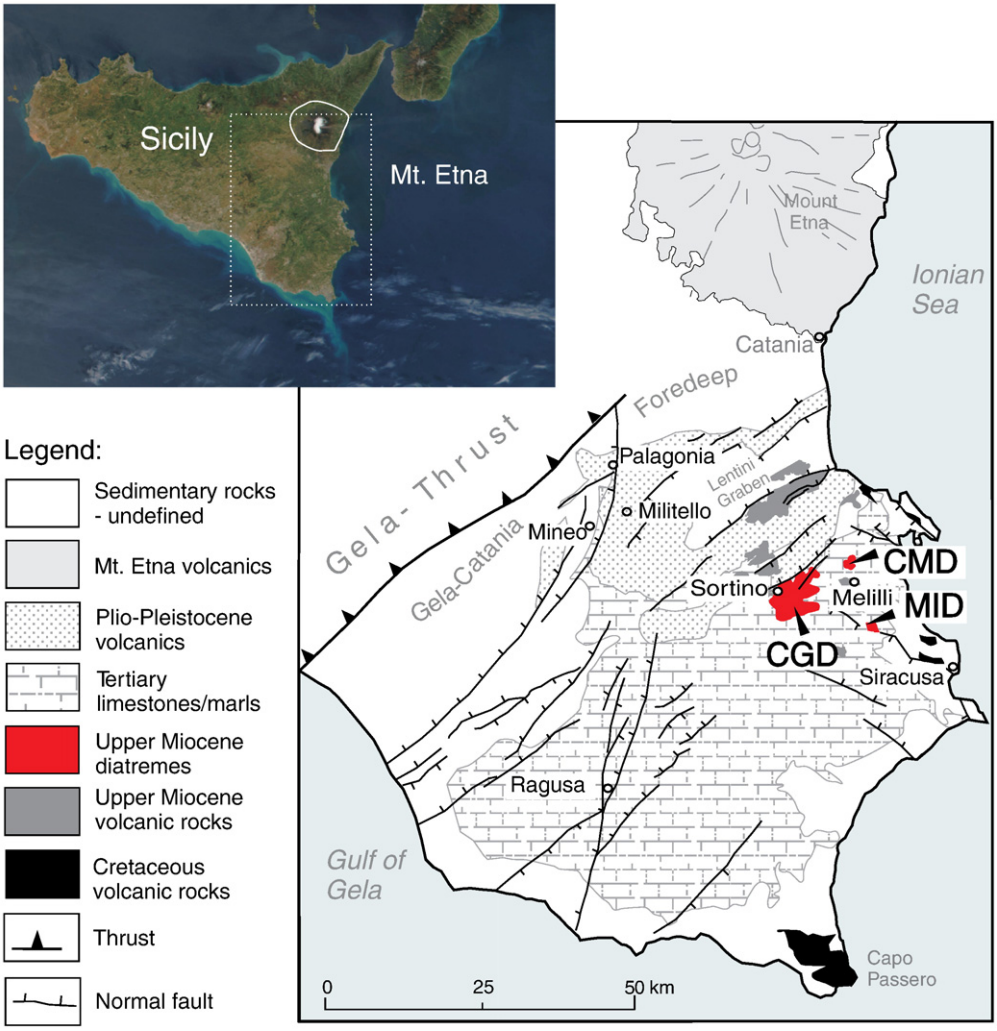

Fig. 1. Setting of the Iblean Plateau and the three best-exposed Miocene diatremes: Costa Giardini diatreme (CGD); 2 Cozzo Molino diatreme (CMD); 3 Mass. D' Ingegna diatreme (MID) (modified from Carbone and Lentini, 1981; Lentini et al., 1986; Adam et al., 2000; Satellite image from NASA/GSFC, MODIS Rapid Response).

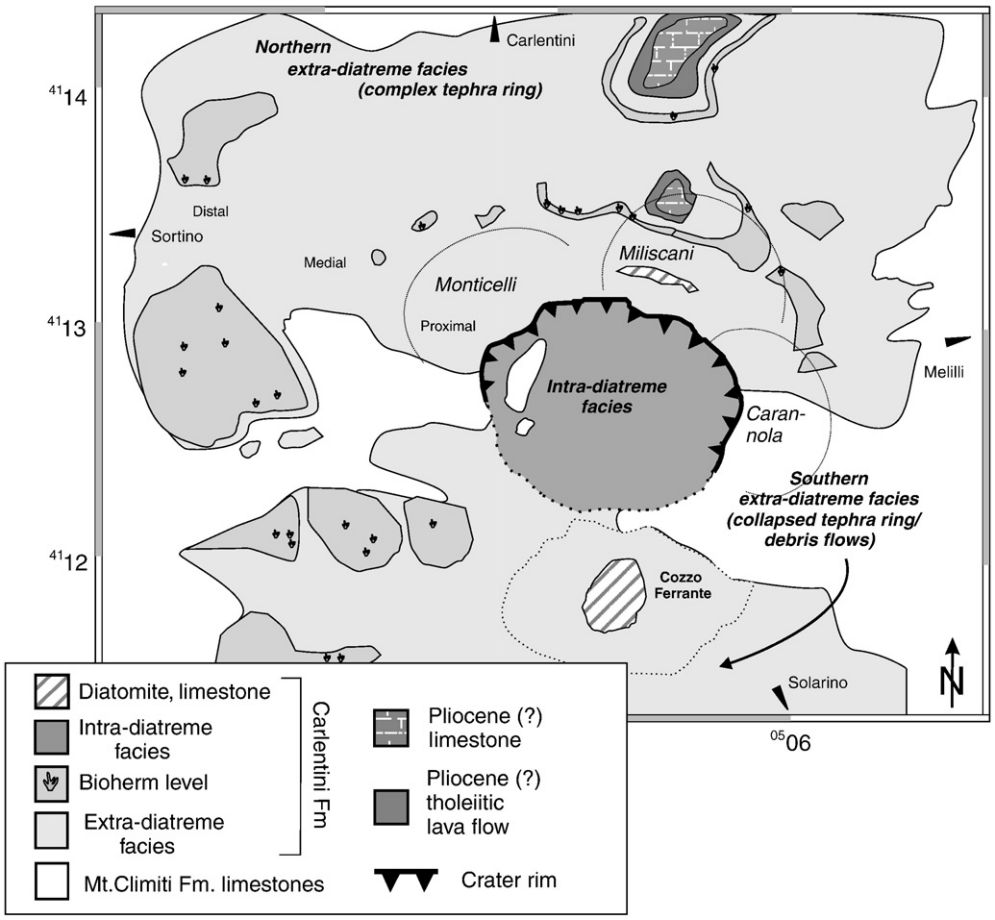

Fig. 2. Schematic map of intra- and extra-diatreme facies at the CGD.

(2) Tachylitic lapilli are moderately to highly vesicular (40 to up to more than 60 vol.%; see Houghton and Wilson, 1989).
(3) Associated pre-diatreme lava flows and hyaloclastites and a final scoria cone indicating that hot magma was able to rise to the surface prior to, and directly following, diatreme formation.

The CGD is also characterized by (1) concentrically and radially-oriented faults and dikes and (2) lack of extensive post-volcanic hydrothermal and/or diagenetic alteration typical for kimberlitic diatremes (Mitchell, 2008).

Glassy spherical and cored juvenile lapilli such as those in the tephra of the Iblean diatremes are the typical juvenile component of kimberlite diatremes and maar-diatreme volcanoes characterized by silica-undersaturated volatile-rich mafic magma (Bailey, 1985; Lloyd and Stoppa, 2003 (and references therein), Sparks et al., 2006; Brown et al., 2008).

In some diatremes these pelletal lapilli have been re-interpreted to form exclusively by phreatomagmatic fragmentation (e.g. Fröhlich, 1978; Lorenz, 1979). There is still no consensus on the nature of the processes leading to formation of these lapilli.

2.2. The shallow marine environment

The Iblean diatremes have unequivocally developed under a permanent water cover in a shallow marine environment as demonstrated by the common abundance of the foraminifer *Amphistegina* sp. in the volcaniclastic sediments. This species indicates water depths of 0–130 m in a reefal or lagoonal environment (Murray, 1991). Intermittent patch reefs subdividing the volcanic sediments of the relic tephra ring encircling the CGD and CMD into two units represent important evidence for one longer hiatus amounting to some 1000 years (see below). The tephra ring is covered by a second complex reef horizon. The CGD was inundated during the entire evolution of the eruptive system. The formation of incipient soil on the top of the tephra ring (Suiting and Schmincke, under review) could simply be the result of growth of the tephra cone above sea level. The soil is overgrown by Porites corals indicating emergence was close to sea level followed by renewed inundation. We cannot exclude small-scale local relative sea-level changes, however (Suiting and Schmincke, under review).

3. Methods

3.1. Geochemical data

Analytical methods used in the analysis of 8 lava samples, mostly from intra-diatreme dikes, are presented elsewhere (Suiting and Schmincke, under review). Whole-rock analyses (XRF) of the CGD lavas (Table 3, Fig. 8) were recalculated on an H_2O and CO_2-free base before plotting in order to allow a comparison between XRF-analyses of slightly altered whole-rock samples with those of fresh glass particles.

3.2. Carbonate bomb

Calcium carbonate concentrations of the matrix of the volcaniclastic sediments were determined using the carbonate bomb technique of Müller and Gastner (1971). The samples were pulverized and afterwards treated with chloridic acid (12%) in the carbonate bomb in order

to measure the gas pressure of CO_2 which increases proportionally to the content of $CaCO_3$.

4. The Costa Giardini diatreme (CGD)

At CGD we distinguish two facies: (1) tephra ring or extra-diatreme facies and (2) diatreme fill or intra-diatreme facies (Fig. 2). The complex northern half of the tephra ring is preserved and exposed in-situ, the southern half is downfaulted and reworked (Fig. 3). We distinguish 5 lithological units in the CGD extra-diatreme facies representing different volcanic phases from at least 4 different horizontally migrating vent locations in the diatreme system: (1) pre-diatreme lava flow and hyaloclastite; (2) submarine to partly emergent tephra cone at Monticelli and initial diatreme formation; (3) Miliscani tephra cone and enlargement of the diatreme; (4) Cozzo Ferrante scoria cone; and (5) post-volcanic phase and collapse (southern tephra facies).

4.1. The pre-diatreme volcanics

A >10 m-thick lava flow with concealed upper and lower contact underlies the town of Sortino and covers an area of at least 4 km^2 in the southern, western and northwestern area outside the diatreme.

Well-bedded hyaloclastite relics (Carannola, Fig. 2) at the eastern rim of the diatreme sharply overlie limestone bedrock. The upper contact to overlying calcareous tephra is erosional. The hyaloclastites are massive or dm-scale layered wacke- to packstones with a carbonate matrix re-crystallized to blocky cement. Lapilli and ash are moderately vesiculated sideromelane (ca. 10 to rarely up to 40 vol.% vesicles) Bedrock fragments from deeper crustal or mantle levels are lacking. Intercalated 2–5 cm-thick re-sedimented layers of lime-mud and hyaloclastic particles imply a calm inter- and post-volcanic depositional environment with suspension flows.

4.2. The calcareous tephra ring

The semi-consolidated CGD tephra consists of a highly variable mixture of glassy (sideromelane to tachylite) juvenile volcanic particles (10–50 vol.%) and various mantle and bedrock xenoliths (10–85 vol.%) mingled into a calcareous matrix (ca. 30–80 vol.% $CaCO_3$ content). At Monticelli, an *upper tephra ring* and *lower tephra ring* reflect two different evolutionary stages (Fig. 4, detailed description see Appendix A). This two-part-division is also found at the CMD. The ca. 22 m-thick CGD *lower tephra ring* is characterized by basal 4 m of a well-mixed lithology of coarse breccia. Lime-mud patches are incorporated into the volcaniclastics containing bedrock blocks (up to 60 cm in diameter) standing on edge (Fig. 5a). The poorly-exposed overlying 18 m-thick lower tephra ring consists of massive poorly-sorted calcareous tephra beds each ca. 1–2 m thick (Fig. 4). Similar beds – interpreted as debris jets (tephra jets/cock's tail jets of Sumita, 1985; Table 2) – still appear in the *upper tephra ring*. Additionally, three general types of primary volcaniclastic deposits (duned layers, carbonate layers and armored lapilli-rich layers; Fig. 5) appear from ca 24 m above base and become increasingly abundant toward the top (Table 2). Channel structures in the uppermost 10 m of the tephra ring (ca 10 vol.% of the upper tephra ring) are interpreted to reflect reworking and downhill sliding of parts of the water-saturated volcaniclastic slurry by debris flows and slumping (Fig. 4).

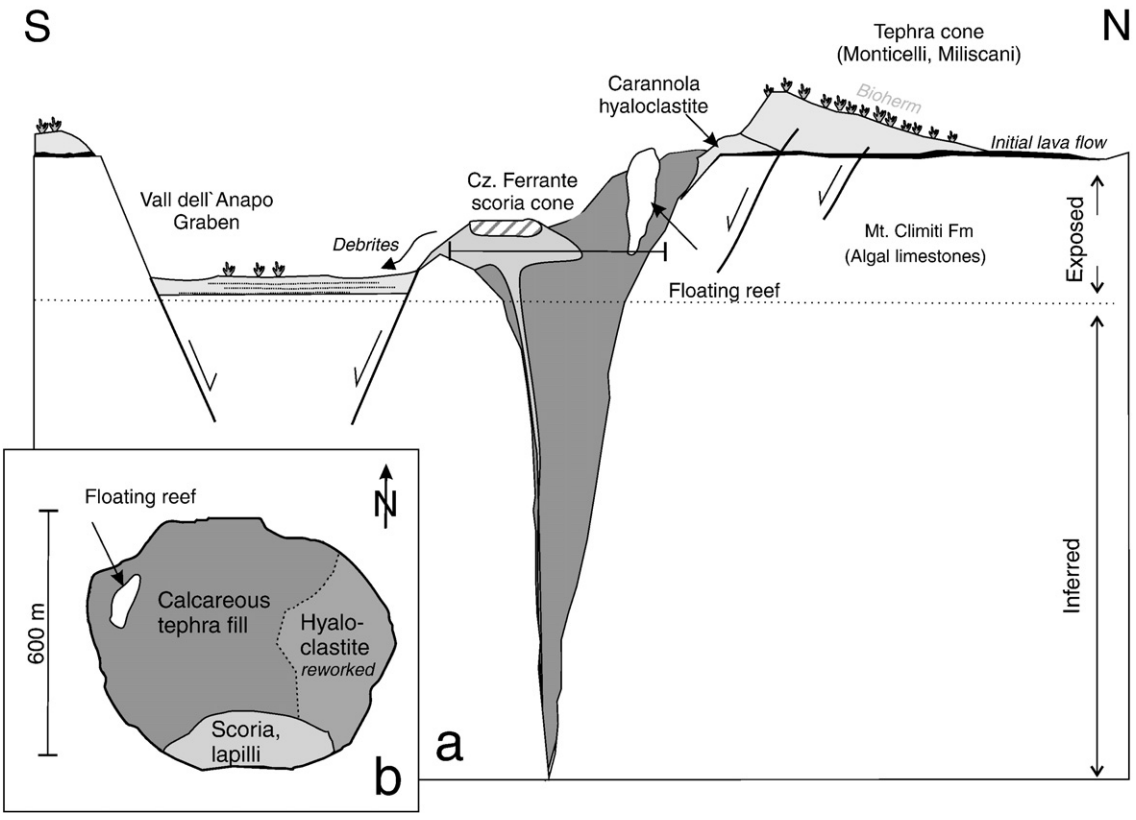

Fig. 3. a) Schematic cross-section of the CGD: A ca. 10 m-thick lava flow and a layered hyaloclastite (Carannola, Fig. 2) underlie the tephra ring. The complex northern tephra ring consists of at least two overlapping tephra cones and is covered by a reef horizon. The southern tephra ring consists of reworked tephra deposited in a graben that formed directly after the end of the eruptions. Diatreme walls are well-exposed in the uppermost 100 m where the diatreme fill had been largely eroded. Large limestone olistoliths (floating reefs) up to 500 m in diameter are part of the fill. A scoria cone at the base of the present diatreme fill represents the final volcanic phase. For legend see Fig. 2. b) Schematic cross-section ca. 150 m below paleo-seafloor.

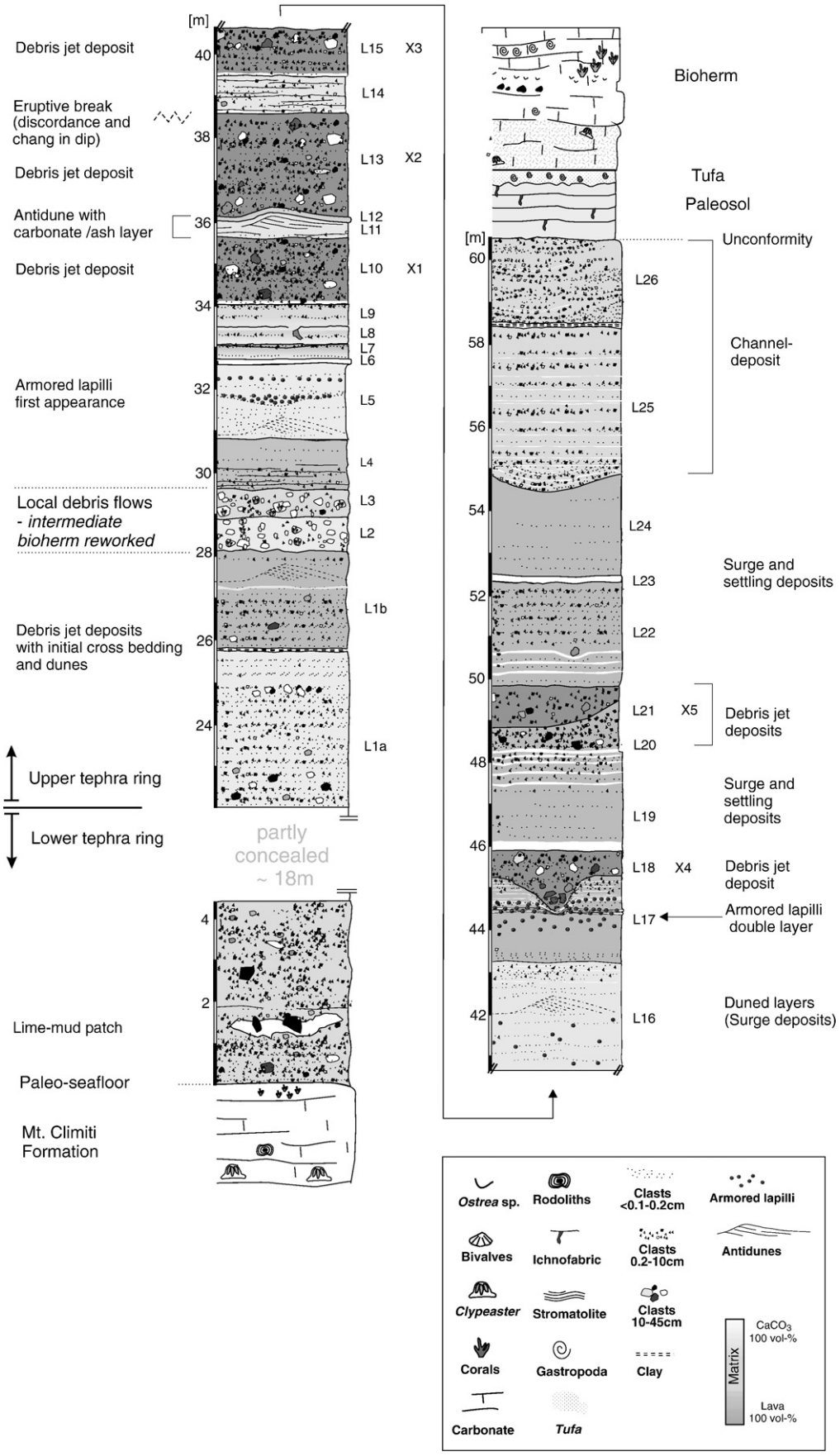

Fig. 4. Monticelli section: Medial facies tephra ring from paleo-seafloor to covering bioherm. The 22 m-thick lower tephra ring of massive poorly-sorted deposits is poorly-exposed. Note large lime-mud patches in the lowermost 2 m of the section. The upper tephra ring (38 m-thick) reveals debris jet deposits alternating with antidune structures, ash/carbonate layers and armored lapilli enriched layers. For legend see inset.

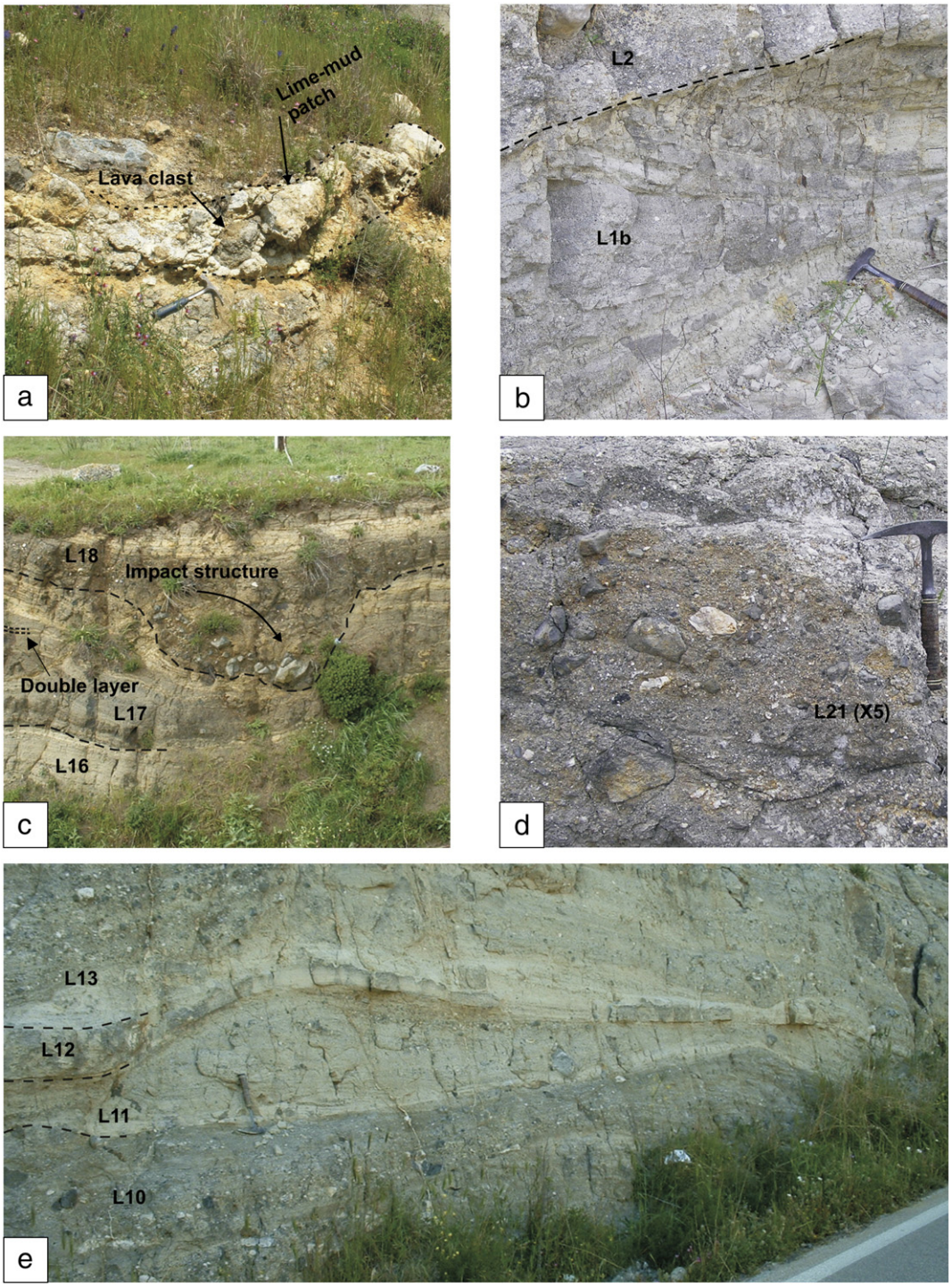

Fig. 5. Characteristic deposits of the extra-diatreme facies at Monticelli: a) Lime-mud patch with lava blocks standing on edge. b) Antidune layer (L1b) with intercalated carbonate horizons and erosive top. c) Impact structure in the upper tephra ring. d) Poorly-sorted lensoid deposit rich in bedrock xenoliths. e) Antidune (L11) covered by carbonate layer (L12), both being sandwiched between two debris jet deposits (L10, L13).

4.3. The southern tephra facies

Ca. 50 m thick, relatively homogenous-layered tephra deposits are exposed in the graben floor of the Anapo River valley (ca. 200 m below the pre-eruptive paleo-seafloor). The polymict deposits are relatively well sorted containing the entire spectrum of bedrock clasts (2 mm to 5 mm in diameter) in a calcareous matrix, larger blocks (up to 40 cm) being rare. Layering varies on a cm to dm-scale. These deposits are interpreted as reworked parts of the CGD tephra and are thought to reflect the post-volcanic collapse of the southern tephra ring and transport of the diatreme fill onto the post-volcanically developing graben plain. Smaller relics of a southern in-situ tephra ring with sedimentologic characteristics similar to the northern tephra ring are exposed on top of the southern graben shoulder ca. 1 km to the south.

4.4. The bioherm level

Biohermal limestones covering the entire CGD tephra ring (Figs. 3 and 4) show all facies characteristics of a micro-atoll that developed on top of the volcanic edifice. These limestones have allowed a detailed

Table 2
Calcareous tephra of the northern extra-diatreme facies at the CGD at Monticelli.

Lithology	Inferred transport processes	Color	Thickness (m)	Textures	Lithoclasts					Juvenile particle		Matrix	
					vol.%	Composition	Size (cm)	Sorting	Roundness	vol.%	Size	vol.%	$CaCO_3$—content (vol.%)
Proximal facies (ca.80 m)													
Massive polymict deposits	Debris jets/tephra jets/ (cock's tail jets of Sumita, 1985), slumping	Light gray	ca. 80	Massive	50	Entire spectrum of bedrock fragments, peridotite and gabbro xenoliths; limestone olistoliths up to 20 m are rare.	0.2–120	Poor	Subangular	20	Lapilli to bomb	30	40
Medial facies (ca. 60 m)													
Bedrock-rich layers (X 1–5 in Figs. 4 and 5d).	Debris jets/tephra jets/ (cock's tail jets of Sumita, 1985)	Gray	1.0–2.5	Massive, local discontinuous layering, erosional unconformities and cross-bedding (antidunes?); drastic thinning away from vent. Ballistically transported bedrock blocks (up to 2 m wide impact sags abundant, blocks shattered during impact).	40	Entire spectrum of bedrock fragments (65 vol.% carbonatic, 25 vol.% basaltic), peridotite and gabbro xenoliths (10 vol.%)	0.05—0.1, max. 25	Poor	Subangular	10	Ash to bomb size	~50	59–63
Duned layers (Fig. 5e, L12)	Base surge, surge (Fisher and Schmincke, 1984)	Buff–yellowish to gray	0.5–0.8	Layering (mm–scale), steeply inclined foreset beds point towards the diatreme and are interpreted as the stoss–side beds of antidunes. The largest antidune at the CGD has a wavelength of ~10 m and an amplitude of ~70 cm. The base is defined by a sharp erosional contact.	10	Entire spectrum of bedrock fragments,	generally <0.2; blocks up to 15 cm in diameter are rare.		Subangular	50	Fine-ash to lapilli: armored lapilli, pelletal lapilli as well as "cored juvenile pelletal lapilli".	40	ca.35
Carbonate layers (Fig. 5b, e)	Settling of suspended lime–mud and ash	White	0.1–0.15	Massive, individual layers (10–15 cm thick) mantle duned layers or tephra jets. Thinner carbonate layers (1–3 cm thick) alternate with volcaniclastic layers.	<10	Entire spectrum of bedrock fragments	<0.5	Good	Subangular	40	Ash/fine-ash	50	69–83
Armored lapilli deposits (Fig. 10f)	Fallout from a turbulent eruption column	Buff-yellow	0.5–0.1	Massive; accretionary and armored lapilli are either distributed in a well-sorted nearly clast-free yellowish carbonate/ash sediment with clast size <3 cm or are concentrated in separate layers such as a characteristic double layer with a calcareous matrix of <10 vol.%. Accretionary and armored lapilli make up as much as 80 vol.% of such layers although the matrix in such layers may also have formed by disintegrated accretionary and armored lapilli.	40	Rim-type armored lapilli (Schumacher and Schmincke, 1995, Section 5.4)	<3	Good	nd	50	Ash to lapilli	10	33–41
Distal facies (ca. 25 m)													
Massive polymict deposits	Debris jets/tephra jets/ (cock's tail jets of Sumita, 1985)	Gray	10–15	Massive	70	Entire spectrum of bedrock fragments	<0.2–20	Poor		~10	Ash to lapilli	20	ca. 50
Duned layers	Surges	Buff-yellow	12	Layered, dune bedding (cm–dm-scale)	85	Rim-type armored lapilli with core of subangular to rounded coralline limestone; rim (ca. 2 mm) of mainly carbonatic material (75 vol.%); entire spectrum of bedrock fragments (<10 vol.%)	Armored lapilli ca. 2 cm; bedrock clasts <3 cm	Good	Armored lapilli round to lenticular; bedrock clasts subangular	~30	Ash/fine-ash	15	ca. 50

reconstruction of the paleo-environment at the CGD (Suiting and Schmincke, under review). Two layers dividing the tephra ring at Monticelli (L2, L3, Fig. 4) contain exclusively poorly-sorted blocks of coralline limestone. These layers may have formed by destruction and reworking of an earlier bioherm. Coral growth during eruptive breaks and thus a hiatus in volcanic activity during the middle of diatreme formation is documented by an in-situ *Porites*-bioherm intercalated in the volcaniclastic sediments at the CMD (Fig. 1). The bioherm was subsequently covered by tephra during renewed volcanic activity.

4.5. The sedimentary diatreme fill

Classically, the diatreme fill of kimberlites is divided into (1) a root zone; (2) a lower facies of reworked massive volcaniclastics with associated dikes; and (3) an upper layered facies (Hawthorne, 1975; Clement and Skinner, 1985; Field and Scott Smith, 1999). Other facies successions are described by Brown et al. (2009).

Layered tephra is missing in the CGD intra-diatreme facies, the uppermost 150 m of the diatreme fill having been eroded. The massive diatreme fill, exposed from ca. 150 m below paleo-seafloor, lithologically greatly resembles the extra-diatreme tephra, but lacks bedding structures. (Fig. 6). The *western* part of the diatreme fill contains bedrock clasts, ultramafic xenoliths and clinopyroxene megacrysts embedded in a calcareous matrix (Fig. 6d and e). Sub-angular to round bedrock clasts (20– 80 vol.%) range from <2 mm to 50 cm in diameter. Irregular to round juvenile basaltic lapilli (10–90 vol.%) are common. Thin lenses of pure carbonate mud are rare. Limestone olistoliths up to 500 m in diameter are also found within the fill. Steeply inclined (ca. 55°) poorly-sorted layers fill the 20 m wide space between the largest olistolith and the diatreme wall (Fig. 6c) at the westernmost internal rim of the diatreme. Bed rock

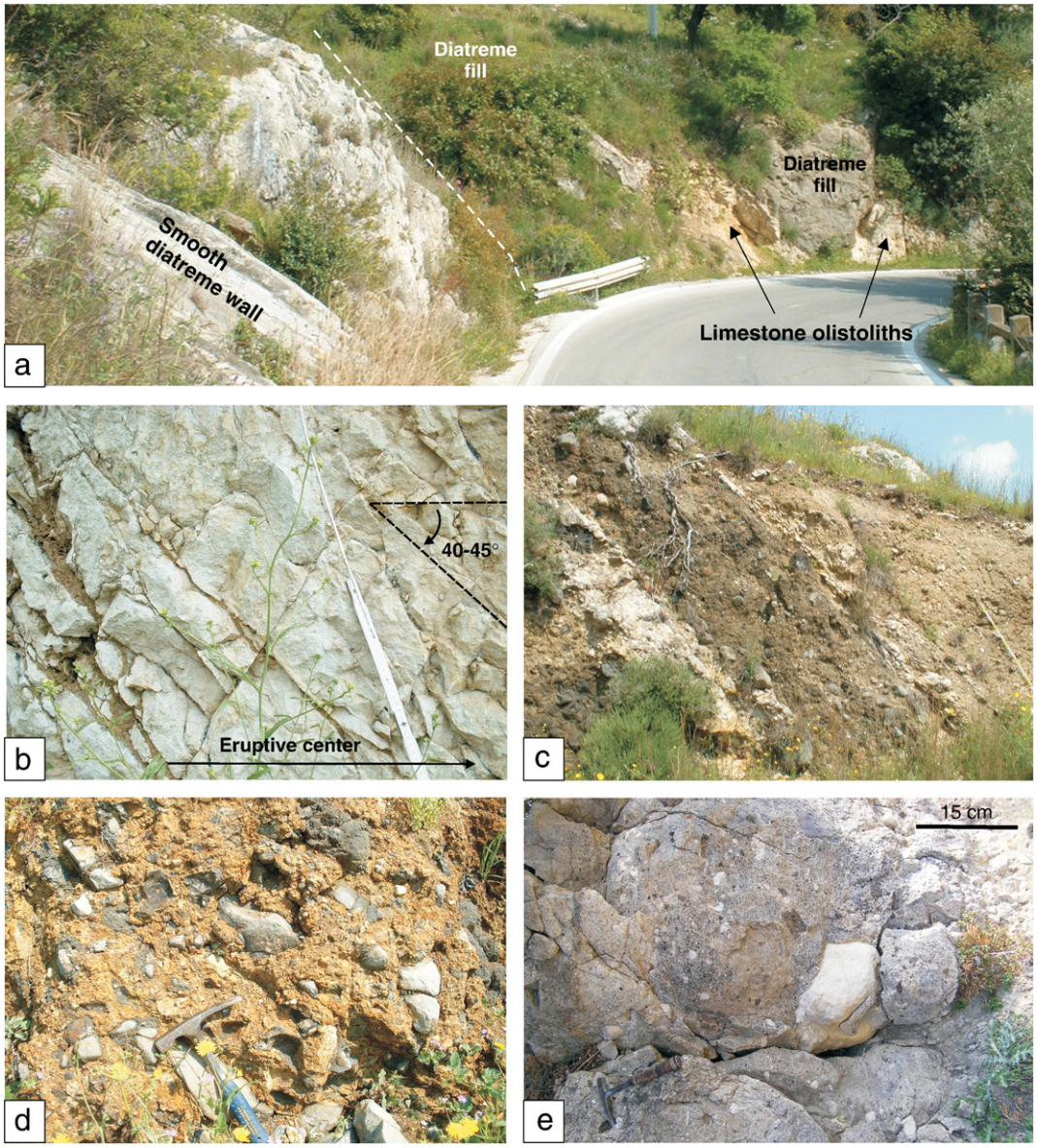

Fig. 6. Characteristic deposits of the intra-diatreme facies: a) Internal rim of the CGD; contact between smooth limestone surfaces and diatreme fill. Limestone olistoliths reflect large blocks of bed rock that have sunk into the diatreme fill. b) Detail of section in the limestone bed rock directly below the smooth inclined surfaces: The bedrock is fractured up to 3 m deep with an increase in clast size inwards. Fault patterns run parallel and perpendicular to the smooth inclined surface of the diatreme wall. The walls are interpreted as relic planes. c) Subvertical layers between diatreme wall and large olistolith. d) Local facies of diatreme fill dominated by reworked lava blocks. e) Typical calcareous diatreme fill with bedrock xenoliths.

clasts (<1 cm to 30 cm in diameter) in these layers are either exclusively round lava or coralline limestone fragments.

The *eastern* diatreme fill is dominated by massive to partly stratified hyaloclastite inclined up to 70° interpreted as part of the initial hyaloclastite cone slumped into the pipe but the area between the western and eastern facies is concealed.

4.6. The late scoria cone complex

Massive reddish oxidized partly agglutinated scoria and lapilli up to 50 m thick – cut by dikes – reflect the southeastern half of a small scoria cone (Cozzo Ferrante cone, Fig. 2). It overlies the reworked calcareous tephra discontinuously. Bedrock and ultramafic xenoliths – abundant in the calcareous tephra facies – are lacking in the final scoria cone. The eastern half of a small (ca. 200 m wide) crater basin is filled with relics of papershale diatomites (Suiting and Schmincke, in prep).

4.7. Diatreme wall

The bedrock of the uppermost 300 m of the CGD consists of Miocene (Aquitanian to Serravalian) algal limestone (Mt. Climiti Fm.; Pedley, 1981) that was already lithified prior to diatreme formation. The limestone diatreme walls show smooth surfaces (each ca. 30–50 m^2) dipping towards the eruptive center at 20° to 40°. In some kimberlite pipe models similar smooth walls are explained by sustained period of gas jet driven erosion (Cas et al., 2008a). At the CGD, evidence suggests fracturing due to decompression. Sets of fractures in the bedrock below the contact to the volcaniclastic fill of the CGD run parallel and perpendicularly to the smooth inclined surfaces (Fig. 6a and b) producing a range of small cube-shaped rock fragments (<10 cm to several m in diameter). The bedrock is locally fractured up to several meters deep with an increase in clast size inwards suggesting decreasing degree of fragmentation. The smooth inclined surfaces are relic planes; rock fragments of varying size produced earlier are now clasts in the fill.

4.8. Fault patterns

The Miocene deformation coincided in time with the onset of volcanism and regional uplift of the central part of the plateau (Grasso pers. comm.). It generated NE–SW-trending faults and grabens in the eastern and northwestern Iblean Plateau (Pedley and Grasso, 1992). At the CGD, a main pre-volcanic normal fault trends northeast–southwest with an offset of 250 m mapped by Lentini et al. (1986) (Fig. 7a). It represents the northern shoulder of a submarine (pull-apart?) graben structure (Suiting and Schmincke, in prep.), the present Anapo river valley.

This main fault is part of a local syn-volcanic system of faults in the Mt. Climiti limestone bedrock that is oriented radially and concentrically with respect to the center of the CGD. These faults define at least 10 concentrically arranged limestone blocks (Fig. 7a and b) that are downfaulted step-wise towards the center of the diatreme. These radial and concentric patterns are also reflected in synvolcanic radial faults in the extra-diatreme volcaniclastic deposits and in thinly bedded limestones of the covering bioherm level at Miliscani. At five localities, 3 to 6 m-thick nephelinitic dikes are oriented radially towards the diatreme. Normal faults in the SW-slope indicate collapse of the volcanic edifice to have taken place following diatreme formation and during growth of the covering bioherm that reveals an enlarged thickness in the lowest blocks in the Anapo river valley.

4.9. Magma composition

The extremely phosphorus-rich nephelinitic magma (SiO_2: 39–41 wt.%; P_2O_5: 2.28–2.86 wt.%) remained remarkably constant compositionally during the entire evolution of the diatreme while volcanic particle types and characteristics of inferred fragmentation and emplacement processes and surficial eruption changed significantly. The composition of the pre-diatreme nephelinite lava flow and the initial hyaloclastite cone is also identical to that of juvenile particles generated during the entire diatreme formation and of late-stage dikes and the final scoria cone (Fig. 8; Table 3).

Round to irregular nephelinitic lapilli from the calcareous tephra ring contain quench crystals of hauyne and apatite. The high initial concentrations of S, F and Cl, are also reflecting high initial overall volatile content, especially CO_2-concentrations of nephelinitic magma as shown by the rare occurrence of calcite lenses in the CGD lavas that we regard as primary, based on textural evidence and high trace element concentrations (e.g. SrO: 0.14–3.51 wt.%; BaO: 0.01–0.02 wt.%). Similar highly SiO_2-undersaturated compositionally mafic lavas also dominate at CMD and MID.

5. Lithic components in the CGD calcareous tephra

5.1. Calcareous matrix

Tephra ring and pipe-filling material consists of up to 40% of carbonate particles (<200 μm) forming the matrix to volcanic clasts. Micritic lime particles make up the fine-grained crystalline part of the matrix. Fragments of corals, fossiliferous limestone, calcareous microfossils (e.g. the foraminifer *Amphistegina* sp.), sea urchin spines and bivalve shells are also mixed into the volcaniclastics. A rough estimate of the volume of $CaCO_3$ in tephra ring and diatreme fill (based on $CaCO_3$ analyses of fine matrix material <200 μm, Table 2) equals the inferred volume of a modeled CGD pipe presuming a ca. 2000 m deep pipe with ca. 0.17 km^3 of excavated bedrock. Thus, we interpret the micritic lime-mud to have mainly – if not entirely – resulted from comminution of the homogenous solidified bedrock limestones rather than representing primary marine sediments existing as lime mud prior to the formation of the diatreme, as also shown by the clean initial hyaloclastite lacking calcareous matrix.

5.2. Bedrock xenoliths

Subangular bedrock clasts (2 mm to rarely ca. 0.8 m in diameter) in the calcareous CGD tephra make up 10 to 60 vol.%. There is no general trend in sorting of clasts, grain size and percentage of relative abundance through the tephra ring. Xenoliths from several stratigraphic levels down to possibly Cretaceous or Jurassic rocks were identified (Fig. 9) from bottom to top of the tephra ring. There is no evidence for the depth of the pipe root zone as walls deeper than 150 m below paleo-seafloor are not exposed. If the dip of the walls does not steepen at depth the diatreme reaches down to at least ca. 500 m below paleo-seafloor. However, Triassic/Jurassic limestone and gabbroic bedrock fragments in the tephra could suggest a depth as deep as 1500 m or more.

5.3. Juvenile volcanic particles

Juvenile lapilli and ash (Table 4) make up 20 to 60 vol.% of the calcareous tephra in both bedded tephra ring and massive pipe facies. Lapilli occur as two different types of glass: transparent sideromelane (ca. 60 vol.%) and opaque tachylite (ca. 40 vol.%). Round to irregular tachylite ash particles seem to be subordinate to irregular to angular sideromelane shards in the ash-fraction. Most juvenile lapilli of the Iblean diatremes contain up to 15 vol.% of quench-crystals, mainly cpx needles or apatite and hauyne. Juvenile particles in the CGD tephra are distinguished from intra-vent recycled juvenile (ash-coated) armored magmatic particles (Houghton and Smith, 1983).

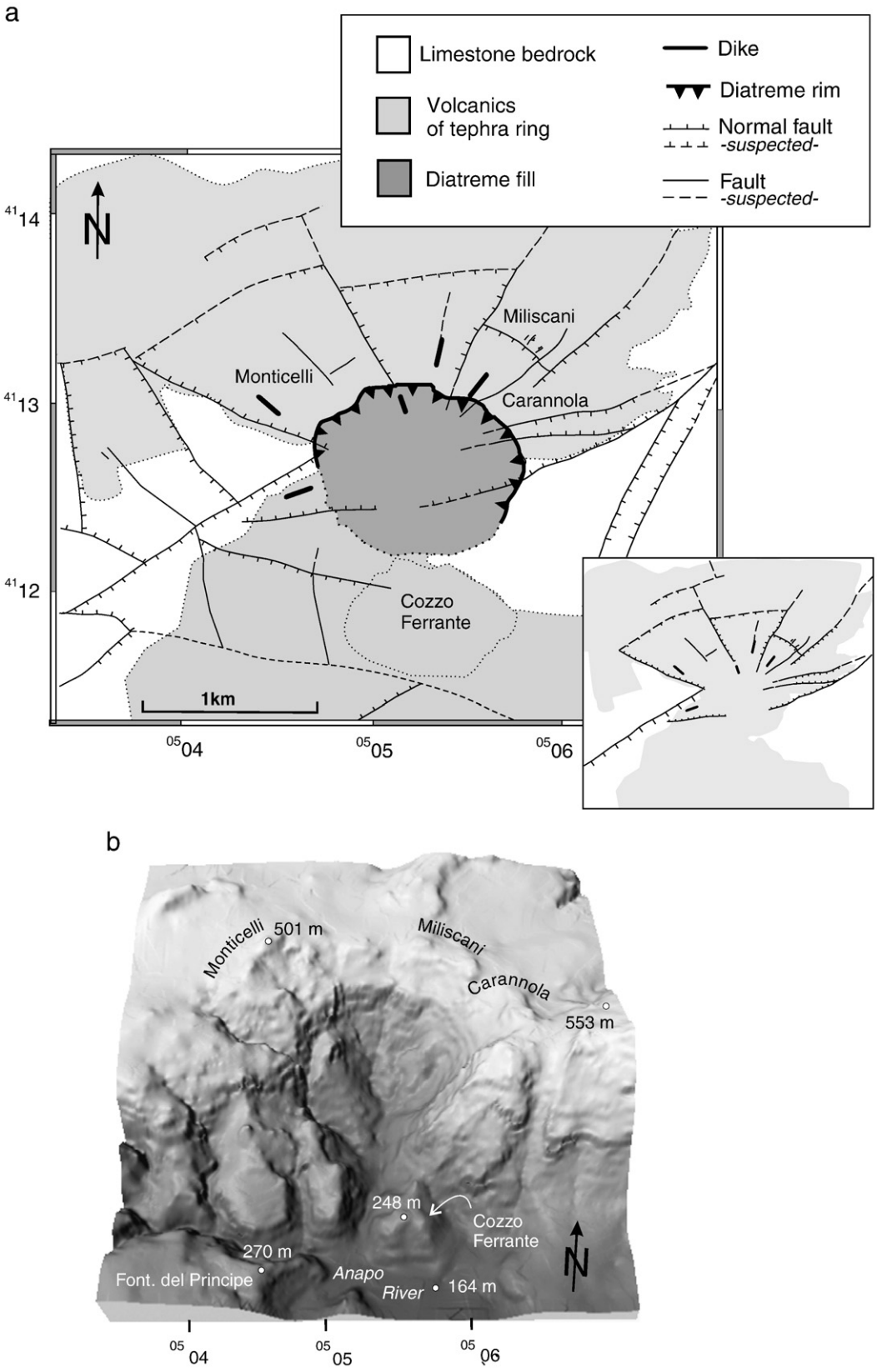

Fig. 7. a) Detailed structural map; insert showing only the radial and concentric fault pattern. b) 3D-elevation model of the CGD showing elevations and main localities.

5.4. Armored lapilli

Armored lapilli (rim-type of Schumacher and Schmincke, 1995; Fig. 10f), ranging in shape from irregular to round or lenticular appear in the upper tephra ring are either distributed in a well-sorted nearly clast-free yellowish sediment with clast size <3 cm or are concentrated in separate layers. Their cores consist of aggregates of coarser limestone or lava particles surrounded by a finer rim of carbonate-

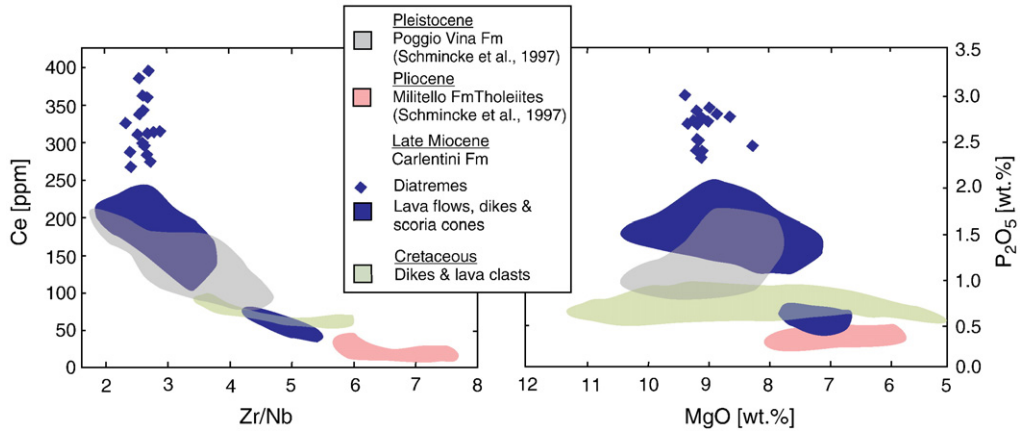

Fig. 8. Characteristic major and trace elements of lavas of the Iblean diatremes compared to other Iblean volcanic rocks (Schmincke et al., 1997; Suiting and Schmincke, under review). Miocene volcanic rocks represent 44 XRF analyses of nephelinitic, alkali basaltic and tholeiitic whole rock samples.

mud and ash. Few (<5 vol.%) xenolithic cores (0.2–5 cm) comprise about 90 vol.% of a lapillus enclosed by a rim (~2 mm) of mainly calcareous material and ash plastered onto it. Multiple rims are rare. Less than 10 vol.% of the armored lapilli are broken. Similar armored lapilli have been described from many kimberlite diatremes (e.g. Lefebre et al., 2008).

5.5. Mantle xenoliths

The CGD mixed tephra contains a wide spectrum of ultramafic (e.g. green clinopyroxenite, black clinopyroxenite, plagioclase-bearing orthopyroxenite, megacrysts of clinopyroxene) and mafic xenoliths (gabbros). Ultramafic xenoliths are especially abundant (up to 10 vol.%) in poorly-sorted lenticular debris jet deposits of the upper tephra ring. These xenoliths vary from <1 cm to more than 20 cm in diameter, some are mantled by lava. The ultramafic and mafic xenoliths of the Iblean diatremes and Valle Guffari (western Iblean Mountains) have been studied by Scribano (1987a,b), Tonarini et al. (1996); Atzori et al. (1999); Punturo et al. (2000); Scribano et al. (2006) and Sapienza et al. (2009).

6. Discussion

6.1. The CGD model

Pre-diatreme domal uplift some time prior to eruption of the initial volcanics is inferred. Concentric and radial fracture patterns (as

Table 3
Major and trace element compositions of the CGD.

Sample		SORT-21	SORT-32	SORT-35	SORT-36	SORT-45	2003-04-04-01	2003 04-04-04	2003 04-06-02
		Dike in the diatreme fill	Lava flow below the top bioherm at Sortino "piscina"	Lava flow at Monticelli	Lava flow top of Cugno Miro	Lava flow at Sortino main road (Via Corso Umberto)	Lava clast in diatreme fill	Lava clast in diatreme fill	Lava pebble in bioherm at Monticelli
SiO_2	%	40.08	40.69	41.27	39.40	41.18	41.53	40.28	39.91
TiO_2	%	1.72	1.65	1.62	1.84	1.59	1.61	1.76	1.79
AL_2O_3	%	12.31	12.47	12.62	12.18	12.44	12.70	12.26	12.27
Fe_2O_3	%	10.86	10.89	11.10	11.03	11.01	11.28	11.00	11.00
MnO	%	0.18	0.18	0.18	0.18	0.17	0.18	0.18	0.17
MgO	%	8.75	8.75	8.88	8.98	8.74	8.93	8.92	8.58
CaO	%	13.78	13.93	13.01	13.62	13.51	13.20	13.26	13.32
Na_2O	%	4.42	3.60	4.27	4.00	4.16	4.43	5.32	4.51
K_2O	%	1.04	1.01	0.97	1.50	0.89	0.96	1.09	1.25
P_2O_5	%	2.62	2.39	2.28	2.86	2.18	2.42	2.73	2.71
Co	ppm	48	52	49	52	50	50	45	50
Cr	ppm	98	109	121	77	128	101	106	86
Ni	ppm	67	66	86	69	92	90	80	73
V	ppm	182	184	182	184	184	191	182	188
Zn	ppm	97	101	101	101	99	100	96	103
Ce	ppm	387	339	343	360	296	326	398	359
La	ppm	236	234	185	268	198	210	211	243
Nb	ppm	103	95	93	109	89	91	102	102
Ga	ppm	17	14	16	16	15	14	17	14
Pb	ppm	5	7	4	6	4	8	4	4
Pr	ppm	45	42	37	59	31	39	51	48
Rb	ppm	35	32	34	30	29	29	35	38
Ba	ppm	1208	1138	1146	1283	1047	1125	1276	1310
Sr	ppm	2901	2991	2562	2979	2592	2621	2785	2981
Th	ppm	21	16	18	19	18	14	14	17
Y	ppm	46	43	40	49	40	42	45	45
Zr	ppm	261	242	240	285	228	212	273	270
H_2O	%	1.48	2.51	1.73	2.73	1.60	1.55	1.02	1.75
CO_2	%	0.49	0.07	0.05	0.05	0.61	0.06	0.11	0.22
SUM	%	98.32	98.74	98.55	99.01	98.65	99.40	98.55	98.11

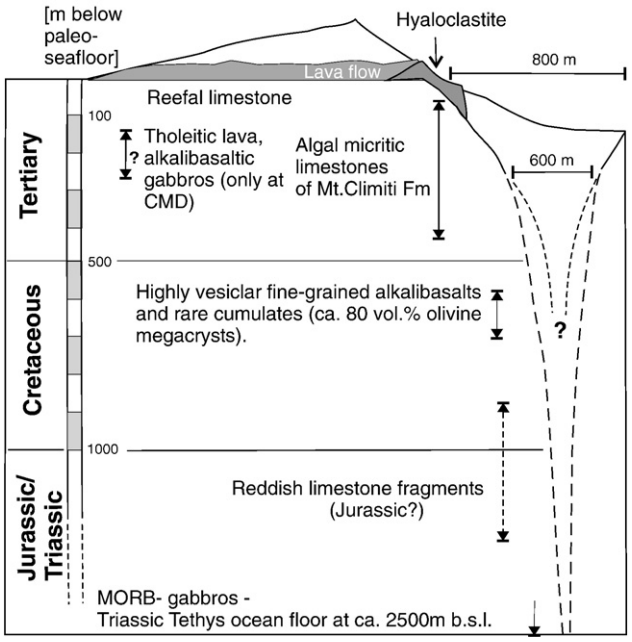

Fig. 9. Stratigraphic levels of identified bedrock types in the Iblean diatreme tephra. Macroscopic distinction and a detailed stratigraphic classification of most included limestone fragments from deeper stratigraphic levels were difficult the underlying Triassic to Jurassic limestones are not exposed in the area but are only known from borehole data (Patacca and Scandone, 1979). MORB-gabbros are interpreted to represent a fossil gabbro ridge from the Paleo Tethys ocean beneath the Iblean Plateau postulated by Scribano et al. (2006).

documented at the CGD at a horizontal scale of 5 to 10 km; Section 4.8) are known from classic model experiments on diatreme emplacement by fluidization (Woolsey et al., 1975) and volcanoes in general (e.g. Nakamura, 1977).

6.1.1. Phase 1 — Precursor lava flow and hyaloclastite cone

The nephelinitic lava flow (Fig. 11) is fine-grained and non-vesicular (already degassed?) and lacks signs of subaqueous emplacement (e.g. pillows). It was subsequently fragmented and reworked in the later volcaniclastics indicating sufficient time to cool down prior to diatreme formation.

The hyaloclastites of the initial phase are interpreted to reflect a Messinian (Suiting and Schmincke, under review) shallow water environment almost free of marine carbonate mud, lacking marine microfossils. We infer an eruptive break between hyaloclastite and diatreme formation based on the sharp upper contact between the "clean" initial hyaloclastite and the lime mud- and bedrock-rich tephra ring (phase 2) and from the observation that a major part of the hyaloclastite has been tilted and partly reworked during diatreme formation.

6.1.2. Phase 2 — Initial diatreme formation (Monticelli vent)

The sudden appearance of calcareous mixed tephra (pulverized bedrock) on top of the lithified but water-covered seabed reflects massive bedrock fragmentation and a dramatic change in fragmentation and emplacement mechanisms (Fig. 11). The initial hyaloclastic eruptions (phase 1) had already generated conduits prior to diatreme formation. Juvenile particles in the calcareous tephra are dominantly spherical tachylite implying pyroclastic fragmentation and possibly transport in a fluidized medium (exsolved volatiles) that allowed surface tensional forces to act on particle formation. The presumed levels of lava and bedrock fragmentation are discussed in Sections 6.3 and 6.4. Xenoliths from all stratigraphic levels were incorporated and comminuted from the onset of the pyroclastic eruption onwards. This is documented in the well-mixed bedrock lithology at the base of the two tephra rings at CGD and CMD. The sudden change from hydroclastic surface eruptions (phase 1) to subsurface pyroclastic bedrock fragmentation of mantle and crustal rocks may have been induced by strong volatile oversaturation and highly explosive CO_2 exsolution during rapid ascent and adiabatic cooling (Kieffer and Delany, 1979; Bailey, 1985; Sparks et al., 2006; Wilson and Head, 2007).

The fluid/particle mixture at the CGD might have exited along the radial fractures, opening the bedrock roof beyond the limited conduit feeding the initial volcanics. Blasts and ballistic transport during the opening phase of the diatreme pipe were the main transport process. This interpretation is also supported by lime-mud patches including bedrock blocks standing on edge implying ballistic transport during early eruptive phases (Fig. 5a). Coalescence and enlargement of the conduits to form a pipe to a larger funnel or vent area by removal of bedrock out of the vent and sinking of bedrock blocks into the funnel. Armored lapilli, ash-coated particles and antidunes in the upper tephra ring imply secondary phreatomagmatic explosions probably during part-emergence of the tephra ring.

The thoroughly mixed diatreme fill is interpreted to have formed by interaction of gravity-induced sinking vs. upward oriented ascent of the two-phase mixture. Fluidization processes would enable large blocks (olistoliths, floating reefs) to sink into the fill during eruptive activity. During and at the end of the eruption, the volcanic conduit was most likely filled with a mixture of lime-mud incorporating bedrock clasts, mantle xenoliths and nephelinitic lapilli. We interpret the volcaniclastic fill as formed synvolcanically as well as by collapse of the eruption column in a deflating system and later debris flows into the crater area. These processes combined with subsidence are thought to be responsible for subvertically inclined layers at the eastern rim of the diatreme (Fig. 6c).

6.1.3. Phase 3 — Diatreme enlargement by vent migration (Miliscani vent)

The relic Miliscani vent is not well-exposed. Sedimentologically, the tephra deposits resemble the Monticelli section. The well-mixed lithology of bedrock xenoliths throughout the entire section of the calcareous tephra implies that the diatreme funnel enlarged at all subsurface levels during this eruptive phase (Fig. 11). The base of the Miliscani cone is characterized by a ca. 10 cm thick layer of fine carbonate mud and ash that sharply overlies the hyaloclastite (Carannola cone). Ash particles of this layer are round to irregular and dominantly highly vesicular. Thus pyroclastic fragmentation processes seem to have dominated initial eruption during this phase.

Several additional phases of vent migration are not preserved because of later collapse and reworking of the entire southern tephra ring. The large olistoliths in the diatreme fill could be relic bedrock walls from between two or more eruptive conduits. The enlarged pipe will have been filled at least partially during eruption and at the end of this eruptive phase. Layered hyaloclastites from the precursory phase partially slumped into the southeastern diatreme funnel. These could represent parts of a collapsing roof area into the enlarging excavated diatreme pipe. Synvolcanic downfaulting of concentrically arranged bedrock blocks enclosing the diatreme fill and subsidence of the diatreme fill itself continued during eruptive breaks and after the main phase of diatreme formation. This is documented in transgressive sections on top of the surrounding bedrock blocks.

6.1.4. Phase 4 — Dike intrusion and scoria cone

The final volcanic phase in the diatreme complex is dominated by radial dike intrusion and fire fountaining with formation of a lapilli/scoria cone (Cozzo Ferrante cone) at the southeastern inner rim of the diatreme (Fig. 11). Dikes and scoria cone do not contain bedrock and ultramafic xenoliths implying that the nephelinitic magma fragmented at the surface during the final stage.

Table 4
Juvenile magmatic particles at the CGD.

	Glass variety	Size	Shape	Vesicularity (vol.%)	Phenocrysts	Phenocrysts (vol.%)	Microcrysts / -needles	Additional features	Interpretation
Pre-cursor hyaloclastite (Fig. 10a)	Sideromelane (95 vol.%)	Ash to lapilli	Angular	10 to 40	ol, ap, hau	5 to 10	cpx	None	Probably degassed melt already enriched in solid phases prior to hydroclastic fragmentation
Pre-cursor hyaloclastite (Fig. 10a)	Tachylite (5 vol.%)	Ash to lapilli	Irregular	10 to 40	ol, ap, hau	5 to 10	nd	None	
Calcareous tephra	Sideromelane	Ash to lapilli	Subangular to irregular	10 to 40	ol>cpx>hau	5 to 10	cpx	Thin mud- or ash-coating covers most sideromelane lapilli	Needles that are not concentrically arranged along the rim and thus do not support any influence of surface tension and rotational forces on their formation. A thin mud- or ash-coating indicates turbulent reworking inside the diatreme or the partly emergent eruption plume. Many of these subangular to irregular sideromelane particles in the CGD tephra are probably rounded reworked lapilli from the initial CGD hyaloclastite.
Calcareous tephra (Fig. 10b,c)	Sideromelane	Lapilli	"Potato"-shaped to spherical	10 to 40	ol>cpx>hau	5 to 10	cpx	Few (<5 vol.%) lapilli are droplet shaped with ol-phenocryst cores	Form strongly influenced by surface tension. Fast cooling (due to adaiabatic decompression or particle/steam contact?) implied.
Calcareous tephra (Fig. 10d, e, g, h)	Tachylite	Lapilli and ash	Round to irregular "potato"-shaped	10 to >60	cpx, ol, hau	5 to 10	cpx	50 vol.% of the pelletal tachylite lapilli are ash-coated armored lapilli.	Form strongly influenced by surface tension and rotation. Slow cooling implied. Ash-coating indicates reworking in a turbulent system inside the diatreme or the partly emergent eruption plume.
Calcareous tephra	Tachylite	Cored lapilli	Round	10 to 40	cpx, ol, rarely hau	5 to 10	cpx	Ca. 10 vol.% of the round cored lapilli contain cores of mainly smaller nephelinitic lapilli rigid enough to retain their identity or xenocrysts derived from fragmented ultramafic xenoliths.	Lapilli appear to be the result of coalescing low-viscosity lava droplets agglutinated around the cores (Fig. 10h), thereby losing their original particle shapes.

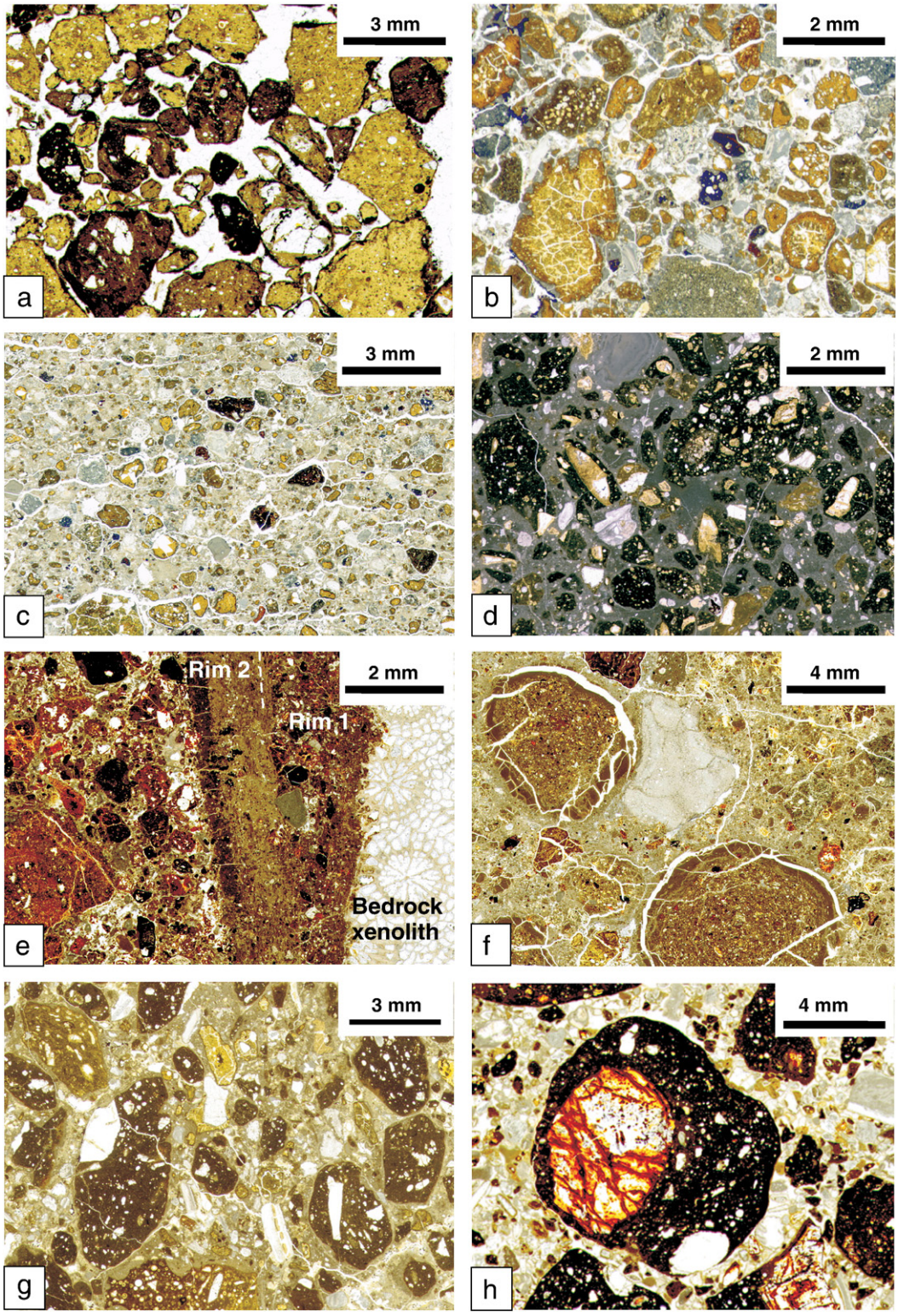

Fig. 10. a) Dominantly angular sideromelane particles from initial hyaloclastite with blocky calcite cement (CGD). b) Potato-shaped sideromelane and tachylite particle from antidune layer at Monticelli (CGD, L1). c) Pelletal to spherical shaped particle from carbonate layer intercalated in duned beds at Monticelli (CGD, L1). d) Ash-coated tachylite particle (multi-cycle evolution) in a calcareous matrix (CMD). e) Detail: ash and lime-mud coated clast of coralline limestone with two generations of rim in an ash/lime-mud matrix. Note round to irregular shape of tachylite ash particles (CGD). f) Armored lapilli from Monticelli road section (L17) in a matrix of lime-mud and ash (CGD). g) Typical mixed volcaniclastic sediment of dominantly round tachylitic and rare irregular sideromelane lapilli in a carbonate matrix from tephra jet layer in basal tephra ring (CMD). h) Round agglutinate tachylite lapilli with a xenolithic core (CMD).

The diatreme wall rock encircles a complex weakness zone of several overlapping eruptive pipes with a round to elliptical shape measuring 800 m in diameter. The ellipse is orientated perpendicularly to the principal NE–SW vector of compression (Barnett and Lorig, 2007): a NE–SW transtensional tectonic setting was established during Late Miocene opening of the Pantelleria rift (Reuther and Eisbacher, 1985).

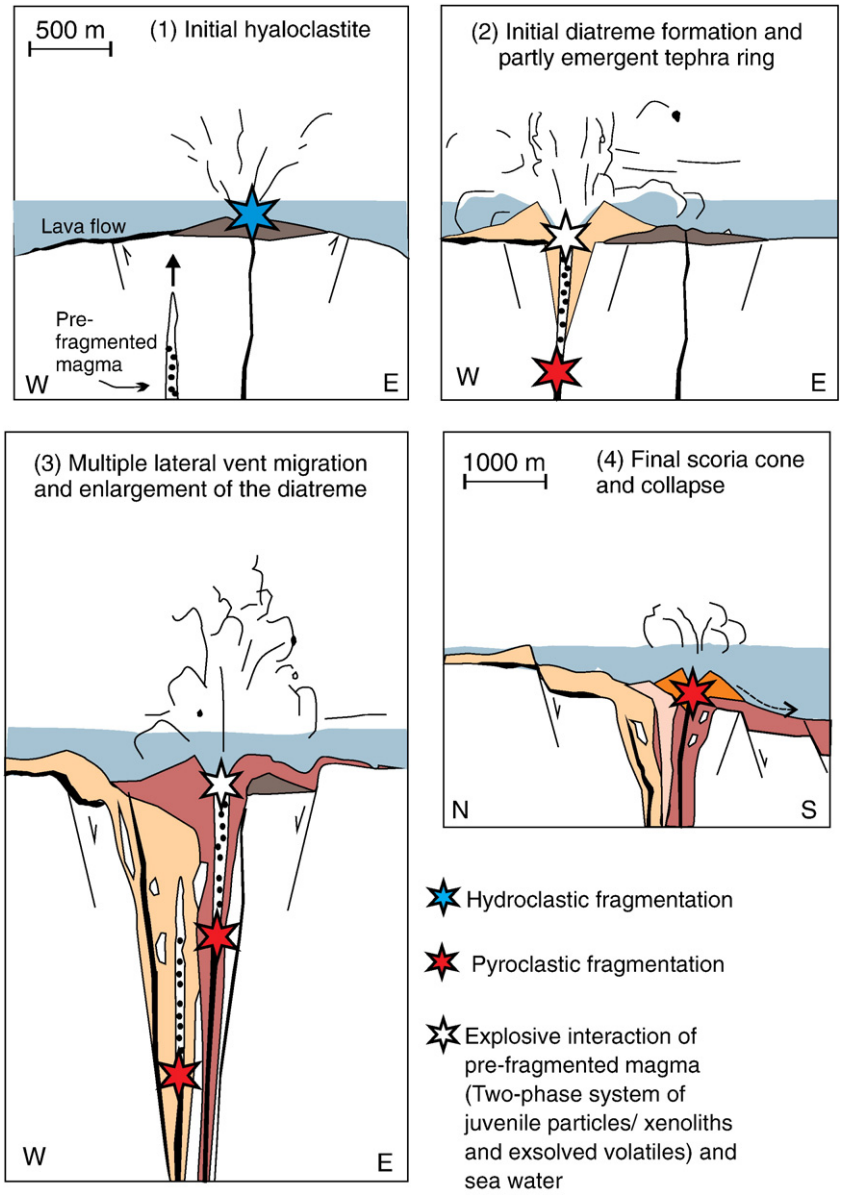

Fig. 11. Evolution of the CGD.

6.1.5. Phase 5 — Post-volcanic sedimentation and collapse

A lagoon developed inside the complex tephra ring encircling the funnel-shaped diatreme. Marine papershale diatomites reflect calm sedimentation in the CGD lagoon. The diatreme must have been almost completely filled at this time.

A post-volcanic submarine (pull-apart?) graben formed along the major NE–SW fault (Section 4.8; Fig. 11). The faulting lead to collapse of the volcanic edifice and massive draining of the diatreme fill onto the newly developing submarine plain. Sedimentologic and structural evidence (Suiting and Schmincke, in prep.) suggests post-volcanic slumping of parts of the scoria cone onto the deepening graben plain.

There are only few signs of post-volcanic and diagenetic alteration in the volcaniclastic sediments: carbonate veins are abundant in the scoria and lapilli cone at Cozzo Ferrante.

6.2. Timing of diatreme formation

The duration of diatreme evolution in general is postulated to range from a few tens of minutes for the formation of a diatreme (Wilson and Head, 2007) to several days to months by Sparks et al. (2006) and Porrit and Cas (2009). At the CMD, a ca. 5 m thick bioherm level of *Porites* patch reefs intercalated in the extra-diatreme tephra ring allows to distinguish several phases of volcanic activity and repose as well as a quantitative estimate of the duration of diatreme formation. The average growth rate of recent *Porites* corals in the Red Sea of ca. 5–7 mm/year (Klein and Loya, 1991) implies that the Miocene reefs would have needed at last 1000 years to grow depending on environmental conditions during volcanic quiescence. We thus conclude that the Iblean diatremes formed during several short eruptive phases with changing vent localities and eruptive breaks lasting at least 1000 years. The total time of diatreme formation may have been several thousand years.

6.3. How did the permanent seawater cover affect diatreme formation?

At the Iblean diatremes, the environmental reconstruction (Section 2.2) shows that most of the eruptive processes took place under shallow submarine conditions. Water depth at the CGD is thought to have been at least 60 m indicated by a paleosol in the Monticelli tephra 60 m above paleo-seafloor (and similar depth estimated at the CMD), shallow enough to allow phreatomagmatic explosions (Fisher and Schmincke, 1984). However, sedimentary structures and juvenile particles of the *lower* tephra ring at the CGD and CMD are not in

harmony with phreatomagmatic fragmentation and transport processes, but suggest deposition from internally generated blasts of carbonate mud consisting of juvenile tachylite particles and bedrock fragments from *all stratigraphic levels*. The initiation of diatreme formation (represented by the first "muddy" bedrock-rich volcaniclastics in the tephra cone) was clearly not due to shallow magma fragmentation, but resulted from highly explosive magma and bedrock comminution on both *deep and shallow* levels. Wilson and Head (2007) argue that magma fragmentation and fluidization in diatremes can result from a downward propagating decompression wave directly after the intrusion has reached the surface.

The onset of explosive interaction of magma (or a volatile/particle mixture) and seawater is documented first by abundant antidune structures and armored lapilli-rich layers in the *upper* tephra rings of the CGD and CMD. Such deposits are characteristic of phreatomagmatic eruptions under subaerial environments (Fisher and Schmincke, 1984). However, pyroclastic processes are still thought to have dominated magma fragmentation because spherical tachylite particles are ubiquitous in antidune and armored lapilli deposits of the upper tephra ring (Section 6.5), while angular sideromelane shards are subordinate or missing. We suggest that the poor vesicularity of these pelletal tachylite lapilli is a result of almost complete degassing of the magma and a concentration of volatiles as fluidizing medium. Tachylite does not reflect a premature stop to degassing due to the interaction of magma and water.

6.4. Deep-seated magmatic fragmentation — a plausible model or wishful thinking?

Tachylitic (slow cooling) spherical lapilli dominate the calcareous tephra of Iblean diatremes. There is no final proof about the deepest level of fragmentation during formation of the Iblean diatremes, but we tentatively suggest that magma and bedrock fragmentation might already have taken place at mantle depth. This idea is supported by:

(1) Xenoliths of mantle origin (rather than bedrock fragments from crustal level) as typical cores of lapilli in the Iblean diatremes suggesting great depth of fragmentation and possibly also lapilli formation. Magmatic processes involved at depth might be e.g. "lift-off" and fast acceleration of the rising melt due to massive CO_2 exsolution passing through the carbonate stability boundary (~80 km depth) and associated fluidization of mantle rocks at this level (Bailey, 1985; Lloyd and Stoppa, 2003).
(2) Round tachylite lapilli that form agglutinated aggregates around xenoliths. In many Eifel maars these are interpreted as documenting their disruption and transport by a fluid/particle mixture of fragmenting low viscosity magma (Schmincke, 2007).

Welding of juvenile particles has not been documented in the calcareous tephra of the Iblean diatremes. It could have been prevented by the overall abundance of carbonate mud in the eruptive system, not allowing direct contact of hot juvenile particles. However, kimberlitic rocks previously interpreted as hypabyssal intrusions (characteristic of diatreme root zones, Wilson and Head, 2007) have recently been reinterpreted to represent welded pyroclastic rocks (Sparks et al., 2006; Brown et al., 2008) implying that hot magmatic fragmentation can definitely take place at least well below the surface.

6.5. Spherical magmatic particles in phreatomagmatic structures — a contradiction?

Spherical particles, however, are the dominant juvenile component in antidunes and armored lapilli-rich layers of the upper tephra ring at the CGD and CMD. These structures suggest transport processes that are commonly associated with phreatomagmatic activity: Eruption columns and plumes with high water/steam content and high amounts of ash/armored lapilli result in pyroclastic density currents that form crossbedded layers by lateral transport. We suggest a model that includes both magmatic fragmentation at depth and secondary shallow magma/water interaction of fluid/particle mixture with abundant sea water inside the diatreme (Fig. 11). This secondary explosive reaction of water and slightly cooled fluid/particle mixture might cause fast cooling and breakup and shedding of low-viscosity lava globules in a turbulent eddy by viscous stretching and surface tension under fast cooling rates. This is described as a viable mechanism for generating fine hydromagmatic tephra from lava globules in cases where mixing is turbulent and water is present (Mastin, 2007).

6.6. CGD in the light of other models of diatreme formation

The entire CGD structure does certainly not result from a single short-lived volcanic event as often postulated for kimberlite diatremes (e.g. Wilson and Head, 2007). Eruptive breaks of at least 1000 years during diatreme evolution are documented in the intercalated bioherms of the Iblean diatremes. The CGD developed as a complex multi-phase succession from volcanic eruptions at different point sources which partially overlap. A combination of internal and external processes as discussed above would enlarge the entire subsurface structure constantly at different depths of the diatreme by bedrock fragmentation and removal, followed by synvolcanic downfaulting of bedrock and subsidence of the diatreme fill of the earlier vents. A multi-phase diatreme evolution has been previously documented from the complex diatreme fill of the K2 pipe in South Africa (Brown et al., 2009), and in larger dimensions from Coombs Hill diatreme complex, Antarctica (White and McClintock, 2001).

Processes of diatreme formation and nephelinitic particles at the CGD contrast with the top down hydroclastic model (Lorenz, 1985; Kurszlaukis and Lorenz, 2008) and the top down pyroclastic model (Sparks et al., 2006). These would imply an enrichment of the stratigraphically youngest bedrock in the basal layers and increasing dominance of older bedrock towards the top of the tephra ring due to downward migration of the explosion level as for example postulated for Hopi Buttes (White, 1991). The Iblean diatremes, however, reveal a well-mixed lithology of bedrock and mantle-xenolith-rich tephra jet deposits throughout all diatreme-forming phases and the general abundance of pyroclastically pre-fragmented round low-vesicular lapilli.

7. Conclusions

(1) Our data suggest that the formation of Miocene shallow marine diatremes on the Iblean Plateau diatremes was governed by a complex interplay of internal and external forcing mechanisms.
(2) Tectonic evolution at the CGD (graben formation in pull-apart motion) is directly linked to formation and collapse of diatreme and tephra ring.
(3) Deep intra-diatreme processes at the Iblean diatremes were clearly internally forced. Direct evidence includes (1) highly silica-undersaturated and extremely phosphorous- and CO_2-rich, low viscosity nephelinitic magma and (2) dominance of irregular to spherical tachylite lapilli and ash, also in phreatomagmatic deposits, moderate to high vesicularity of particles formed by surface tension during diatreme evolution (concentrically shelled lapilli). Indirect evidence includes abundance of mantle xenoliths in the tephra ring deposits. We favor a model of pre-fragmentation of magma at depth due to massive CO_2 exsolution.
(4) External forcing at the CGD was provided by the abundance of seawater, which led to hydroclastic explosions at shallow diatreme levels. Magma-water interaction was probably not responsible for most of magma fragmentation or for deep diatreme processes.
(5) A combination of both internal and external factors may characterize diatreme formation in general. Their relative importance in diatreme formation may largely depend on environmental conditions and not on the magma composition and nature of the driving force of the eruption.

Acknowledgements

Our study was supported by grants from the Deutsche Forschungsgemeinschaft (Schm 250/79-1 and 81-1, 2). We dedicate this paper to the late Mario Grasso (Catania), pioneer of Iblean geology. Mario provided crucial logistic support and aided our work in many ways. We appreciate constructive comments by two anonymous reviewers.

Appendix A. Supplementary data

Supplementary data associated with this article can be found, in the online version, at doi:10.1016/j.jvolgeores.2009.07.013.

References

Adam, F., Reuther, C.-D., Grasso, M., Torelli, L., 2000. Active fault kinematics and crustal stresses along the Ionian margin of southeastern Sicily. Tectonophysics 326, 217–239.
Atzori, P., Mazzoleni, P., Punturo, R., Scribano, V., 1999. Garnet-spinel-pyroxenite xenoliths from the Hyblean plateau (South Eastern Sicily, Italy). Mineralogy and Petrology 6, 215–226.
Bailey, D.K., 1985. Fluids, melts, flowage and styles of eruption in alkaline ultramafic magmatism. Transactions of the Geological Society of South Africa 88, 449–457.
Barnett, W.P., Lorig, L., 2007. A model for stress controlled pipe growth. Journal of Volcanology and Geothermal Research 159, 108–125.
Bednarz, U., Schmincke, H.-U., 1990. Evolution of the Quaternary melilite–nephelinite Herchenberg volcano (East Eifel). Bulletin of Volcanology 52, 426–444.
Brown, R.J., Buse, B., Sparks, R.S.J., Field, M., 2008. On the welding of pyroclasts from very low-viscosity magmas, examples from kimberlite volcanoes. Journal of Geology 116, 354–374.
Brown, R.J., Tait, M., Field, M., Sparks, R.S.J., 2009. Geology of a complex kimberlite pipe (K2 pipe, Venetia Mine, South Africa): insight into conduit processes during explosive ultrabasic eruptions. Bulletin of Volcanology 71, 95–112.
Carbone, S., Lentini, F., 1981. Caratteri deposizionali delle vulcaniti del Miocene superiore negli Iblei (Sicilia sud-orientale). Geologica Romana 20, 79–101.
Cas, R.A.F., Hayman, P.C., Pittari, A., Porritt, L.A., 2008a. Some major problems with existing models and terminology associated with kimberlites from a volcanological perspective, and some suggestions. Journal of Volcanology and Geothermal Research 174, 209–225.
Cas, R.A.F., Porritt, L.A., Pittari, A., Hayman, P.C., 2008b. A new approach to kimberlite facies terminology using a revised general approach to the nomenclature of all volcanic rocks and deposits: descriptive to genetic. Journal of Volcanology and Geothermal Research 174, 226–240.
Clement, C.R., 1982. A comparative geological study of some major kimberlite pipes in the Northern Cape and Orange Free State. Ph. D. thesis, Univ. Capetown, South Africa, 432 pp.
Clement, C.R., Reid, A.M., 1989. The origin of kimberlite pipes: an interpretation based on a synthesis of geological features displayed by southern African occurrences. Geological Society of Australia Special Publications 14, 632–646.
Clement, C.R., Skinner, E.M.W., 1985. A textural–genetic classification of kimberlites. Transactions of the Geological Society of South Africa 88, 403–409.
Dawson, J.B., 1980. Kimberlites and their Xenoliths. Springer, New York. 252 pp.
Field, M., Scott Smith, B.H., 1999. Contrasting geology and near-surface emplacement of kimberlite pipes in southern Africa and Canada. Proceedings of the 7th International Kimberlite Conference 1, 214–237.
Fisher, R.V., Schmincke, H.-U., 1984. Pyroclastic Rocks. Springer, New York. 472 pp.
Fröhlich, G., 1978. Dampfexplosionen durch Kontakt zwischen Wasser und heißen Schmelzen. Chemie Ingenieur Technik 50, 861–866.
Grasso, M., Lentini, F., Pedley, H.M., 1982. Late Tortonian-Lower Messinian (Miocene) paleogeography of SE Sicily: information from two new formations of the Sortino group. Sedimentary Geology 32, 279–300.
Hawthorne, J.B., 1975. Model of a kimberlite pipe. Physical and Chemical Earth 9, 1–15.
Hearn, B.C., 1968. Diatremes with kimberlitic affinities in North Central Montana. Science 159, 622–625.
Houghton, B.F., Smith, R.T., 1983. Recycling of magmatic clasts during explosive eruptions: estimating the true juvenile content of phreatomagmatic volcanic deposits. Bulletin of Volcanology 55, 414–420.
Houghton, B.F., Wilson, C.J.N., 1989. A vesicularity index for pyroclastic deposits. Bulletin of Volcanology 51, 451–462.
Kieffer, S.W., Delany, J.M., 1979. Isentropic decompression of fluids from crustal and mantle pressures. Journal of Geophysical Research 84, 1611–1620.
Klein, R., Loya, Y., 1991. Skeletal growth and density patterns of two Porites corals from Gulf of Eilat, Red Sea. Marine Ecolology Progress Series 77, 253–259.
Kurszlaukis, S., 1998. On the first experimental phreatomagmatic explosion of a kimberlite melt. Journal of Volcanology and Geothermal Research 80 (3–4), 323–326.
Kurszlaukis, S., Lorenz, V., 2008. Formation of "Tuffisitic kimberlites" by phreatomagmatic processes. Journal of Volcanology and Geothermal Research 174, 68–80.
Kurszlaukis, S., Büttner, R., Zimanowski, B., Lorenz, V., 1998. On the first experimental phreatomagmatic explosion of a kimberlite melt. Journal of Volcanology and Geothermal Research 80, 323–326.
Lefebre, N.S., Fulop, A., Kurszlaukis, S., 2008. Variance in juvenile accretionary pyroclasts of the Attawapiskat kimberlites: implications for eruption dynamics and interpretation of volcanic processes from drill core. 9th International Kimberlite Conference, Frankfurt a. M., Germany, Extended abstracts, 9IKC-A-00315.
Lentini, F., Carbone, S., Cugno, S., Grasso, M., Scamard, G., Sciuto, F., Ferrara, V., 1986. Carta geologica della settore nord-orientale Ibleo (Sicilia SE), scale 1:50.000. Società Elaborazioni Cartografiche, Florence.
Lloyd, F.E., Stoppa, F., 2003. Pelletal lapilli in diatremes — some inspiration from the old masters. Geolines 15, 65–71.
Lorenz, V., 1979. Phreatomagmatic origin of the olivine melilitite diatremes of the Swabian Alb, Germany. In: Boyd, F.R., Meyer, H.O.A. (Eds.), Kimberlites, Diatremes and Diamonds, Their Geology, Petrology and Geochemistry: Proceedings of the Second International Kimberlite Conference 1, pp. 354–363.
Lorenz, V., 1985. Maars and diatremes of phreatomagmatic origin: a review. Transvaal Geological Society of South Africa 88, 459–470.
Lorenz, V., Kurszlaukis, S., 2007. Root zone processes in the phreatomagmatic pipe emplacement model and consequences for the evolution of maar- diatreme volcanoes. Journal of Volcanology and Geothermal Research 159, 4–32.
Mastin, L.G., 2007. Generation of fine hydromagmatic ash by growth and disintegration of glassy rinds. Journal of Geophysical Research 112, B02203. doi:10.1029/2005JB003883.
Mitchell, R.H., 2008. Petrology of hypabyssal kimberlites: relevance to primary magma compositions. Journal of Volcanology and Geothermal Research 174, 1–8.
Müller, G., Gastner, M., 1971. The "Karbonat-Bombe", a simple device for the determination of the carbonate content in sediments, soils and other materials. Neues Jahrbuch für Mineralogie, Monatshefte 10, 466–469.
Murray, J.W., 1991. Ecology and palaeoecology of benthic foraminifera. InLongman Scientific & Technical, England, pp. 316–322.
Nakamura, K., 1977. Volcanoes as possible indicators of tectonic stress orientation — Aleutians and Alaska. Pure and applied geophysics 115, 87–112.
Patacca, E., Scandone, P., 1979. Mesozoic paleotectonic evolution of the Ragusa zone (southeastern Sicily). Geologica Romana 18, 331–369.
Pedley, H.M., 1981. Sedimentology and paleoenvironment of the southeast Sicilian Tertiary platform carbonates. Sedimentary Geology 28, 273–291.
Pedley, M., Grasso, M., 1992. Miocene syntectonic sedimentation along the western margins of the Hyblean-Malta platform: a guide to plate margin processes in the central Mediterranean. Journal of Geodynamics 15, 19–37.
Porrit, L.A., Cas, R.A.F., 2009. Reconstruction of a kimberlite eruption, using an integrated volcanological, geochemical and numerical approach: a case study of the Fox Kimberlite, NWT, Canada. Journal of Volcanology and Geothermal Research 179, 241–264.
Punturo, R., Kern, H., Scribano, V., Atzori, P., 2000. Petrophysical and petrological characteristics of deep-seated xenoliths from the Hyblean Plateau, south-eastern Sicily: suggestions for a lithospheric model. Mineralogica Petrographica Acta 43, 1–20.
Reuther, C.-D., Eisbacher, G.-H., 1985. Pantelleria rift — crustal extension in a convergent intraplate setting. Geologische Rundschau 74, 585–597.
Sapienza, G.T., Griffin, W.L., O'Reilly, S.Y., Morten, L., 2009. Petrology and Sr–Nd–Hf isotope geochemistry of gabbro xenoliths from the Hyblean Plateau: a MARID reservoir beneath SE Sicily? Contribution to Mineralogy and Petrology 157, 1–22.
Schmincke, H.-U., 2007. The Quaternary volcanic fields of the east and west Eifel (Germany). In: Ritter, R., Christensen, U. (Eds.), Mantle Plumes – A Multidisciplinary Approach. Springer, Heidelberg, pp. 241–322.
Schmincke, H.-U., Behncke, B., Grasso, M., Raffi, S., 1997. Evolution of the northwestern Iblean Mountains, Sicily: uplift, Pliocene/Pleistocene sea-level changes, paleoenvironment and volcanism. Geologische Rundschau 86, 637–669.
Schumacher, R., Schmincke, H.-U., 1995. Models for the origin of accretionary lapilli. Bulletin of Volcanology 56, 626–639.
Scribano, V., 1987a. Deep-seated xenoliths in alkaline volcanic rocks from the Hyblean Plateau (SE-Sicily). Memorie della Società Geologica Italiana 38, 475–482.
Scribano, V., 1987b. The ultramafic and mafic nodule suite in a tuff-breccia pipe from Cozzo Molino (Hyblean Plateau, Sicily). Rendiconti della Società Italiana di Mineralogia e Petrologia 42, 203–217.
Scribano, V., Sapienza, G., Braga, R., Morten, L., 2006. Gabbroic xenoliths in tuff-breccia pipes from the Hyblean Plateau: insights into the nature and composition of the lower crust underneath south-eastern Sicily, Italy. Mineralogy and Petrology 86, 63–88.
Skinner, E.M.R., Marsh, J.S., 2004. Distinct kimberlite classes with contrasting eruption processes. Lithos 76, 183–200.
Sparks, R.S.J., Baker, L., Brown, R.J., Field, M., Schumacher, J., Stripp, G., Walters, A., 2006. Dynamical constraints on kimberlite volcanism. Journal of Volcanology and Geothermal Research 155, 18–48.
Suiting, I., 2004. The evolution of the "Costa Giardini" Diatreme (Monti Iblei, Sicily): stratigraphic, volcanic, structural, compositional and paleoenvironmental. Diplomarbeit (Ma Thesis), Univ. Kiel, Germany.
Sumita, M., 1985. Ring-shaped cone formed during the 1983 Miyake-jima Eruption. Bulletin of the Volcanological Society of Japan 30, 11–32.
Tonarini, S., D'Orazio, M., Armienti, P., Innocenti, F., Scribano, V., 1996. Geochemical features of eastern Sicily lithosphere as probed by Hyblean xenoliths and lavas. European Journal of Mineralogy 8, 1153–1173.
White, J.D.L., 1991. Maar-diatreme phreatomagmatism at Hopi Buttes, Navajo Nation (Arizona), USA. Bulletin of Volcanology 53, 239–258.
White, J.D.L., McClintock, M.K., 2001. Immense vent complex marks flood basalt eruption in a wet, failed rift: Coombs Hills, Antarctica. Geology 29 (10), 935–938.
Wilson, L., Head, J.W., 2007. An integrated model of kimberlite ascent and eruption. Nature 447, 53–57.
Woolsey, T.S., McCallum, M.E., Schumm, S.A., 1975. Modeling of diatreme emplacement by fluidization. Physics and Chemistry of the Earth 9, 29–42.